**Thermal Decomposition Reaction and a High Temperature Kinetic Model of Dimethyl Ether**

Zhao, Z., Kazakov, A., and Dryer, F. L.
*Mechanical and Aerospace Engineering, Princeton University, Princeton, NJ 08540*

**Introduction**

As a result of its high cetane number and low sooting characteristics, dimethyl ether (DME) has been proposed as a promising alternative diesel fuel and fuel additive for reducing particulate and NOx emissions. Several experimental and theoretical studies have considered DME oxidation and pyrolysis characteristics previously. Recently, a detailed kinetic mechanism [1,2] and its updated version [3] of DME oxidation and pyrolysis has been developed based on comparisons with data from the Princeton Variable-Pressure Flow Reactor (VPFR) over a temperature range of 550-850K at the pressures of 12-18 atm. The model was also compared against results from a jet-stirred reactor [4] and a shock-tube [5]. More recently, Kaiser et al. [6] and McIlroy et al. [7] successfully used compared the model predictions with species profiles measured in low or atmospheric pressure, premixed, burner stabilized flames. However, the model ability to predict laminar flame speeds has been questioned [8,9]. More importantly, since the development of the DME model [1,2], significant advances in fundamentals (mechanistic issues, thermochemical and kinetic parameters) have occurred particularly for $H_2/O_2$ and $C_1$-$C_2$ kinetics, which are important at flame conditions. As a result, we have embarked upon updating the high temperature aspects of the DME pyrolysis and oxidation model to reflect the changes in the small molecule and radical kinetics and thermochemistry.

The DME molecular decomposition reaction is significant at flow reactor, shock tube and laminar flame conditions. Since the decomposition and abstraction pathways are coupled during both pyrolysis and oxidation, accurate description of the DME unimolecular decomposition process over a wide range of conditions is needed to further understand the contributions of the abstraction reactions in comprehensive kinetic models describing high temperature DME combustion. In the present work, thermal decomposition of DME was studied theoretically and the updated high temperature pyrolysis and oxidation model was compared with literature experimental data.

**Dimethyl Ether Unimolecular Decomposition**

During DME pyrolysis, initiation proceeds via unimolecular decomposition: $CH_3OCH_3 = CH_3 + CH_3O$ (R1). The rate constant for the unimolecular decomposition of DME was investigated theoretically based on RRKM/master equation approach. Initially, all of the competitive reaction channels were considered, but their rate constants were found to be are much lower than $k_1$, and only become competitive at very high temperatures (above 3000 K). As a result, only the dominant channel, i.e. reaction (R1) was considered in further detail in the present study. Equilibrium geometries of the reactants and products were optimized by the hybrid density functional B3LYP method [10-13] with the 6-31G(d) basis set. Vibrational frequencies, calculated using the same method were scaled by a factor of 0.96 [14]. Energies were computed at G3B3 level of theory [14]. The Gaussian 98 package [15] was used for all the molecular orbital calculations. We also compared the energy barriers (including a Zero-Point Energy (ZPE) correction at 0 K) calculated by different theoretical methods, as well as available experimental results. We found that all theoretical results are in a reasonable agreement with one another. In particular, the energy barrier obtained in the present study matches very well the recent *ab initio* results of Nash and Francisco [16]. Similar to Li et al. [17], special consideration was given to the two hindered rotations around $CH_3$-internal rotors to evaluate the rotational potentials and to compute the density of states.

The rate constants for the DME unimolecular decomposition were computed using an in-house computer code [17]. The microscopic rate coefficient for simple-fission reaction (R1) was evaluated using the prescribed high-pressure limit for this channel and the molecular properties of reaction products. The high-pressure limit rate constant was calculated from microscopic reversibility using a rate expression of $2.75\times10^{13}$ $cm^3$/mol/s for the reverse reaction, recombination of $CH_3O$ and $CH_3$. We estimate the rate expression in the reverse direction, as the recombination of two radical species has no associated activation energy and the *A*-factor normally varies between $1 - 3\times10^{13}$ for similar reactions [18-20]. The molecular parameters (reaction barriers, moments of inertia, and vibrational frequencies) are required as input for the sum and density-of-states computations, followed by the microscopic rate constant $k(E)$ calculation based on the RRKM theory [21]. With the input information for the collision model, rate constants were calculated after solving the master equations [21]. The in-house computer program was specifically designed for computational efficiency (thus allowing extensive parametric studies without sacrificing the accuracy). These features include arbitrary energy and temperature dependence of $\langle \Delta E_{down} \rangle$ (see below), a more rigorous treatment of hindered rotations, and evaluation of microscopic rate coefficients for loose transition states from the prescribed high-pressure-limit rate constant.

The energy increment was fixed at 1 $cm^{-1}$ in all sum and density-of-states computations. The standard form of the exponential-down model was used for collision energy transfer. In the absence of reliable measurements in the falloff region that are normally used to calibrate the collision model, the model parameters had to be assigned *a priori*. Specifically, following recommendations of Knyazev and Slagle [22] based on their extensive comparisons of theoretical predictions with the large body of experimental data, and accounting for both temperature and energy dependencies of the main collision model parameter, the energy transfer per downward collision, $\langle \Delta E_{down} \rangle$, were calculated using the following expression, $\langle \Delta E_{down} \rangle = A T E^{1/2}$, where $T$ is the temperature, $E$ is the internal energy, and $A$ is an adjustable constant taken as $4.313\times10^{-3}$ and $3.458\times10^{-3}$ $cm^{-1/2}K^{-1}$ for $N_2$ and Ar respectively in the present study. This calculation yields a value of about 217 and 174 $cm^{-1}$ for $N_2$ and Ar at 298 K, which was determined experimentally for similar

reaction by Knyazev and Tsang [23] and the energy corresponding to the barrier of reaction (R1). The collision frequency of DME with the bath gas was estimated from the Lennard-Jones parameters adopted from Kee et al. [24]. An energy grain size of 10 $cm^{-1}$ was used in the master equation solutions, and the resulting matrix size was 7410×7410. This grain size provided numerically convergent results for all temperatures and pressures considered in this study.

The calculated rate constants of reactions (R1) over the temperature range 500 - 2500 K at 1 atm are presented in Figure 1. The rate constant agrees well with the experimental data of Batt et al. [25] by utilizing a $\langle \Delta E_{down} \rangle$ of 300 $cm^{-1}$ at 298K for DME, which is consistent with the experimental work of Knyazev and Tsang [23] for similar species. The rate constant at high-pressure limit is in very good agreement with the measurement of Pacey [26]. However, the present theoretical work gives a value significantly lower than the experimental data reported in [27, 28]. In order to fit the data in [27,28], a rate constant of at least (1-2)×$10^{14}$ has to be assigned to the reverse reaction of R1, which is much higher than that of similar reactions obtained experimentally, e.g. [18-20], and theoretically [29]. High values of R1 are also inconsistent with the empirical "geometric mean rule", e.g. [30-32], which provides an estimate for the recombination rate coefficient of two radicals, A and B, $k_{AB} = 2(k_{AA} k_{BB})^{1/2}$, based on self-recombination rate coefficients $k_{AA}$ and $k_{BB}$ for A and B. respectively. By using experimental values for recombination of $CH_3$ + $CH_3$ [33-35] and $CH_3O$ + $CH_3O$ [36], one obtains a rate coefficient of about 2×$10^{13}$ for the rate coefficient of R1, i.e. a factor of 5-10 lower than the values needed to match the experimental data of [27-28].

The present rate coefficient at around 800 K is higher than the experimental data of [25] by utilizing a $\langle \Delta E_{down} \rangle$ of 269 at 298K for $CH_4$ as bath gas (the value was recommended in [23]). By assigning either a rate constant of 1.35×$10^{13}$ to the reverse reaction of R1, or a $\langle \Delta E_{down} \rangle$ of 175 at 298K, the calculated rate constant fits the data well. Even so, under all conditions, the present analysis results in a rate coefficient at 1 atm that is much lower (a factor of 3 at 1000 K) and exhibits a higher degree of falloff than that obtained by Curran et al. [2].

**High Temperature Model for Dimethyl Ether Pyrolysis and Oxidation**

A high temperature decomposition and oxidation model was updated to reflect the recent advances in small molecule and radical kinetics and thermochemistry, to incorporate the new unimolecular decomposition results described above, and to re-evaluate recent predictions of DME laminar flame speed measurements. The chemical kinetic reaction mechanism consists of 263 reversible elementary reactions and 46 species. The $H_2$, $C_1$-$C_2$ submodel is based on an ethanol mechanism recently developed in our laboratory against extensive experimental data [37-38]. The DME high temperature subset contains reactions with $O_2$ as well as the thermal decomposition as initiation steps. As the radical pool becomes established, H atom abstraction from the fuel becomes more important. These propagation reactions involve radicals (e.g., H, O, OH, $HO_2$, $CH_3$, $CH_3O$) reacting with the fuel. The methoxymethyl radical ($CH_3OCH_2$) is formed by H-atom abstraction from DME. Its reactions include a thermal decomposition reaction forming formaldehyde and $CH_3$, and reactions with $O_2$, $HO_2$, O, OH, $CH_3$, and $CH_3O$. Among the H atom abstraction reactions, the reaction of fuel with methyl radical is important for describing fuel consumption at flow reactor conditions and for ignition delay at shock tube conditions. The limited literature data for this reaction are all restricted to low temperatures (<=1000 K). We performed a least square modified Arrhenius fit based on the experimental data of [25-26, 28, 39]. This new correlation exhibits strong temperature dependence, similar to the theoretical work of Wu et al. [40], although their rate is consistently lower than the experimental data and the present result by about a factor of 3. The present recommendation is a factor of 1.4 higher than that recommended by Curran et al. [2] at 1000 K.

The H abstraction from DME by OH is also an important reaction affecting the fuel consumption. Tranter and Walker [41] studied the reaction experimentally at a 753 K and their data is consistent with another recent experimental work [42] conducted at 295-660 K. The rate constant correlation presented by Tranter and Walker [41] was used in the present mechanism and it exhibits stronger temperature dependence than that used by Curran et al. [2]. Tranter and Walker [41] also studied the H abstraction from DME by H and this rate correlation was also adopted in the present mechanism. It is about a factor of 1.5 higher than the one used in the model of Curran et al. [2].

The termination reaction between formyl and methyl radical HCO + $CH_3$ = CO + $CH_4$ (R2), is also an important reaction in the DME oxidation/pyrolysis system, since the existing of large amount of HCO and $CH_3$ radical. The rate constant in the original Curran et al [2] model is 1.20×$10^{14}$ $cm^3$/mol/s. This value is close to the collision limit and likely exceeds high-pressure limit for this reaction; actual rate coefficient at high temperature will be even lower due to falloff effects. In the present mechanism, we used the rate constant of 2.65×$10^{13}$ $cm^3$/mol/s recommended by Mulenko [43], which is same as the one used in GRI-Mech 3.0 [44].

**Model Predictions against Experimental Data**

The high temperature DME mechanism described above was compared with pyrolysis and oxidation experiments in the VPFR as well as the other experimental data. Figures 2-3 show species profiles from VPFR experiments [2] against model predictions. The model predicts well the VPFR oxidation data [2] for major species (e.g., DME, $O_2$, CO, $H_2O$) and even for trace intermediates (e.g., methane, and propene) at stoichiometric (Fig. 2) and lean condition. For the fuel rich and pyrolysis (Fig. 3) cases, the agreement with fuel/oxygen consumption remains; however, minor species and intermediates are predicted with less satisfactory than with Curran et al.'s model.

Sensitivity analysis was performed to determine the reactions that strongly influence the DME pyrolysis /oxidation system. Figure 4 shows the important reactions for $H_2O$, $CH_4$ and $CH_2O$ with their sensitivity coefficients calculated

when 80% fuel is consumed for $\phi = 3.16$ case at 1 atm. Under these conditions, the concentration of these species are all very sensitive to fuel decomposition, the reaction of fuel with methyl radical, and several other reactions with methyl radical, such as, $2CH_3$ (+ M) = $C_2H_6$ (+ M) (R3), $CH_2O + CH_3 = CH_4 + HCO$ (R4), $CH_3 + HO_2 = CH_4 + O_2$ (R5), $CH_3 + HO_2 = CH_3O + OH$ (R6), and reactions related to formaldehyde oxidation sub-mechanism.

The chemical kinetic mechanism was also used to simulate the experimental shock tube results of [4] at a temperature range of 1200 – 1600 K and 3.5 Bar. Figure 7 shows the comparison of the predicted peak [CO]×[O] with the experimentally observed ignition delay times (based on light emission from the reaction of CO with O atoms). Good agreement between prediction and experiment is achieved for all equivalence ratios, although predicted values are somewhat larger at lower temperatures. Similar behavior was observed in Curran et al.'s original modeling and the literature model for allene and propyne [48]. Both predicted and experimental ignition delay times decrease at lean conditions. The ignition delay time is also very sensitive to the fuel dissociation reaction, (R1) and to several reactions involved with methyl radical and formaldehyde (Fig. 5).

The chemical species profiles have been measured for burner-stabilized flames at atmospheric pressure for DME/air using gas chromatography or Fourier transform infrared (FTIR) spectroscopy [6], or for DME/Ar at low-pressure (4.00 kPa) using a molecular beam mass spectrometer (MBMS) and laser-induced fluorescence (LIF) [7]. As shown in Fig. 6 for the low pressure flame, the model performs well in reproducing the major stable species, such as, DME, $O_2$, CO, $CO_2$, $H_2O$, and $H_2$. Minor species such as $CH_4$ and $CH_2O$ are also well predicted by the model. The predicted and measured acetylene ($C_2H_2$) profile shapes are in good agreement, but the magnitude of the experimental data is significantly higher than that predicted. For the OH radical, the model reproduces well the shape of the OH profile, however, discrepancies are observed at post-flame equilibriums. This disagreement most likely is caused by OH calibration in the LIF experiments, where the values from equilibrium calculations were used to calibrate OH. Recently, Ruscic et al. [45] studied the heat of formation of OH radical both experimentally and theoretically, and the recommended value of 8.91 kcal/mol at 298 K is in excellent agreement with the recent experimental result of 8.92 kcal/mol [46]. The heat of formation value presented by Ruscic et al. [45] was used in the current mechanism. It is significantly different than the one from CHEMKIN [47] database, which was likely being used in the LIF calibration. Actually, by replacing the OH thermochemical data back to the value of CHEMKIN database, the model well predicts the OH concentration at equilibrium (Fig. 5). Fig. 7 shows the comparison of the species profiles for the DME/air flames at atmospheric pressure. Again, a generally good agreement between model and experiment was observed for major species, such as DME, $O_2$, CO and $CO_2$. The intermediate species, such as $C_2H_4$ and $C_2H_6$, were also correctly reproduced by the model. Some minor deficiencies exist for $CH_2O$ and $CH_4$.

The comparison for laminar premixed flame speeds at room temperature and different pressure are in Fig 9-10. Similar to other fuels (e.g. [9]), the experimental data exhibit significant scatter (average of 19% in differences). For example, the laminar flame speed of $CH_4$ has an average difference of 20% within the very recent literature data, including the two sets of data from the same groups who made DME measurements. The laminar flame speed data from our previous study [49] appear consistently higher than these from literature [8-9,50]. The present model reproduces well the laminar flame speed at atmospheric pressure, however, the difference became significant at higher pressures. The sensitivity spectrum for DME/air flames is similar for all the pressures and it exhibits the features typically seen and well documented for flames of small hydrocarbons, and the results are qualitatively similar to those in Curran et al. [2] model. Figure 11 shows the sensitivity results for laminar flame speed at 10 atm and 298 K. The spectrum is dominated by the main chain branching reaction, $H + O_2 = OH + O$ (R7), formyl decomposition, $HCO + M = CO + H + M$ (R8), and CO oxidation, $CO + OH = CO_2 + H$ (R9). The reactions that are specific to DME contribute noticeably are only the unimolecular decomposition of DME, $CH_3OCH_3 = CH_3 + CH_3O$ (R1), and H abstraction from DME by H atom, $CH_3OCH_3 + H = CH_3OCH_3 + H_2$ (R10),

While it is possible to further impro internal.tgzve the agreement between the model predictions and the present data by adjusting less established rate coefficients, the present agreement appears to be acceptable for a majority of the model uses. Modifications in kinetics and thermochemistry should not be performed based upon improving this agreement without investigating the result of the changes in predictions of fundamental kinetics observations used in initially validating the mechanism and against flame speed measurements for other simple fuels.

**Summary**

A high temperature DME pyrolysis and oxidation model based on a hierarchical nature of reacting systems to reflect the new development in the small molecule and radical kinetics and thermochemistry has been developed. Thermal decomposition of DME was studied theoretically by using the RRKM/master equation approach and the high temperature model was then compared with the literature experimental data. The new model predicts well the high temperature flow reactor data, high temperature shock tube ignition delays, and the species profiles from the burner-stabilized flames. Predictions of laminar flame speed also reasonably agree with the available experimental data. The sensitivity analysis suggests the need for further model refinement for reactions involving C1 level sub-mechanism, especially formaldehyde oxidation.

**Acknowledgements**

This work was supported by the Chemical Sciences, Geosciences and Biosciences Division, Office of Basic Energy Sciences, Office of Science, U.S. Department of Energy under Grant No. DE-FG02-86ER13503. We also want to acknowledge Dr. H. Curran for helpful discussion.

**References**


1. Fischer, S.L., Dryer, F.L., and Curran, H.J. (2000). *Int. J. Chem. Kinet.*, **32**: 741-759.
2. Curran, H.J., Fischer, S.L., and Dryer, F.L. (2000). *Int .J. Chem. Kinet.*, **32**: 741-759.
3. Curran, H.J. (2004), *Personal communication*.
4. Dagaut, P., Daly, C., Simmie, J.M., and Cathonnet, M. (1998). *Symp. Int. Combust.*, **27**: 361-369.
5. Pfahl, U., Fieweger, K., and Adomeit, G. (1996). *Symp. Int. Combust*. **26**: 781-789.
6. Kaiser, E.W., Wallington, T.J., Hurley, M.D., Platz, J., Curran, H.J., Pitz, W.J., and Westbrook, J. (2000). *J. Phys. Chem. A*, **104**: 8194-8206.
7. McIlroy, A., Hain, T.D., Michelsen, H.A., and Cool, T.A. (2000). *Proc. Combust. Inst.*, **28**: 1647-1653.
8. Daly, C.A., Simmie, J.M., Würmel, J., Djebaïli, N., and Paillard, C. (2001). *Combust. Flame*, **125**: 1329-1340.
9. Qin, X., Ju, Y. (2004). *Symp. Int. Combust.*, **30**.
10. Becke, A.D. (1988). *Phys. Rev. A* **38**, 3098.
11. Becke, A.D. (1993). *J. Chem. Phys*. **98**, 5648.
12. Lee, C., Yang, W., and Parr, R.G. (1988). *Phys. Rev. B* 37, 785.
13. Stephens, P.J., Devlin, F.J., Chabalowski, C.F., and Frisch, M.J. (1994). *J. Phys. Chem.* 98, 11623.
14. Baboul, A.G., Curtiss, L.A., Redfern, P.C., and Raghavachari, K. (1999). *J. Chem. Phys*. 110, 7650.
15. Frisch, M.J., Trucks, G.W., Schlegel, H.B., Gill, P.M.W., Johnson, B.G., Robb, M.A., Cheeseman, J.R., Keith, T., Petersson, G.A., Montgomery, J.A., Raghavachari, K., Al-Laham, M.A., Zakrzewski, V.G., Oritiz, J.V., Foresman, J.B., Cioslowski, J., Stefanov, B.B., Nanyakkara, A., Challacombe, M., Peng, C.Y., Ayala, P.Y., Chen, W., Wong, M.W., Andres, J.L., Replogle, E.S., Gomperts, R., Martin, R.L., Fox, D.J., Binkley, J.S., Defrees, D. J., Baker, J., Stewart, J.P., Head-Gordon, M., Gonzalez, C., and Pople, J.A. (1998). Gaussian, Inc., Pittsburgh, PA.
16. Nash, J.J., and Francisco, J. S. (1998). *J. Phys. Chem. A*, **102**: 236.
17. Li, J., Kazakov, A., Dryer, F.L. (2004a). *J. Phys. Chem. A* **108** (38): 7671-7680.
18. Forst, W. (1991). *J. Phys. Chem*. 95, 3612.
19. Du, H., Hessler, J.P., and Ogren, P.J. (1996). *J. Phys. Chem*. 100, 974.
20. Pesa, M., Pilling, M.J., Robertson, S.H., and Wardlaw, D.M. (1998). *J. Phys. Chem. A* 102, 8526.
21. Gilbert, R.G., and Smith, S.C. (1990). Blackwell Scientific Publications, Oxford, U.K.
22. Knyazev, V.D., and Slagle, I.R. (2001). *J. Phys. Chem. A* 105, 3196.
23. Knyazev, V.D., and Tsang, W. (2000). *J. Phys. Chem. A* 104 (46): 10747-10765.
24. Kee, R.J., Dixon-lewis, G., Warnatz, J., Coltrin, M.E., and Miller, J.A. (1986). *Sandia Report SAND86-8246*, Sandia National Laboratories, Albuquerque, NM.
25. Batt, L., Alvarado-Salinas, G., Reid, I.A.B., Robinson, C., and Smith, D.B. (1982). *Proc. Combust. Inst.* **19**: 81-87.
26. Pacey, P.D. (1975). *Can. J. Chem.* **53**: 2742-2747.
27. Aronowitz, D., and Naegeli, D. (1977). *Int. J. Chem. Kinet.*, **9**: 471-479.
28. Held, A.M., Manthorne, K.C., Pacey, P.D., and Reinholdt, H.P. (1977). *Can. J. Chem.* **55**: 4128-4134.
29. Harding, L.B. (2004). DOE, BES 25th Annual Combustion Research Conference, Warrenton, VA.
30. Kerr, J.A. Trotman-Dickenson, A.F.(1961). Prog. React. Kinet., Pergamon Press, Oxford, 1961, pp. 105-129.
31. Gerland, L. J., and Bayes, K.D. (1990). *J.Phys. Chem.* **94**: 4941-4945.
32. Knyazev, V.D., Slagle, I.R., and Bryukov, M.G., (2003). *J.Phys. Chem. A*, **107**: 6558-6564.
33. Pagsberg, P., Munk, J., Sillesen, A., and Anastasi, C.(1988). *Chem. Phys.* Lett., **146**.
34. Wang, B., and Fockenberg, C. (2001). *J. Phys. Chem. A*, **105**: 8449 – 8455.
35. Cody, R.J., Payne, W.A., Jr., Thorn, R. P., Jr., Nesbitt, F.L., Iannone, M.A., Tardy, D.C., and Stief, L.J. (2002). *J. Phys. Chem. A*, 106: 6060 – 6067.
36. Barker, J.R.; Benson, S.W.; Mendenhall, G.D.; Goldern, D.M. (1977). *U.S. NTIS PB Rep.*
37. Li, J.; Zhao, Z.; Kazakov, A.; Dryer, F. L. (2004b). *Int J Chem Kinet*, **36**: 566-575.
38. Li, J.; Zhao, Z.; Kazakov, A.; Dryer, F. L.; Scire, J. J., Jr. (2004c). *Int J Chem Kinet*, Submitted.
39. Arthur, N.L., Gray, P., and Herod, A.A. (1969). *Can. J. Chem.* **47**.
40. Wu, J.Y., Liu, J.Y., Li, Z.S., Huang, X.R., and Sun, C.C. (2003). *J. Comp. Chem*. **24** (5): 593-600.
41. Tranter, R.S., and Walker, R.W. (2001). *Phys. Chem. Chem. Phys.*, **3**: 4722-4732.
42. Bonard, A., Daele, V., Delfau, J.L., and Vovelle, C. (2002). *J.Phys. Chem. A*, **106**: 4384-4389.
43. Mulenko, S.A. (1987). *Rev. Roum. Phys.* 32:173.
44. Smith, G.P., Golden, D.M., Frenklach, M., Eiteneer, B., Goldenberg, M., Bowman,C.T., Hanson, R.K., Song, S., Gardiner Jr., W.C., Lissianski, V.V., and Qin, Z. (1999). http://www.me.berkeley.edu/gri_mech/.
45. Ruscic, B., Wagner, A.F., Harding, L.B., Asher, R.L., Feller, D., Dixon, D.A., Peterson, K.A., Song, Y., Qian, X.M., Ng, C.Y., Liu, J.B., and Chen, W.W. (2002). *J. Phys. Chem. A*, **106**, 2727.
46. Herbon, J.T., Hanson, R.K., Golden, D.M., and Bowman, C.T. (2002). *Proc. Combust. Inst.* **29**: 1201-1209.
47. Kee, R.J., Rupley, F.M., and Miller, J.A. (1989). *SAND89-8009*, Sandia National Laboratories, Albuquerque, NM.
48. Curran, H., Simmie, J.M., Dagaut, P., Voisin, D.,and Cathonnet, M., (1996). *Proc. Combust. Inst.*, **26**: 613-620.
49. Zhao, Z. (2002). MSE Thesis, MAE Department, Princeton University, Princeton, NJ.
50. Law, C.K., and Jomass, G. (2004). *Personal communication*.

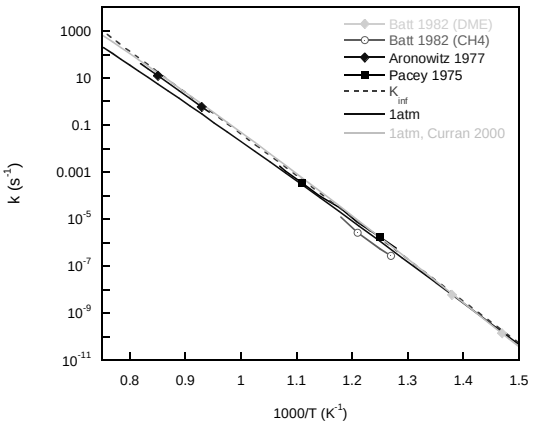


Figure 1: Rate constant of the reaction $CH_3OCH_3 = CH_3 + CH_3O$.

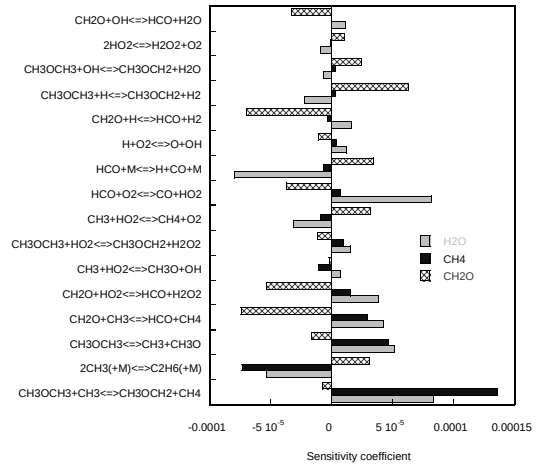


Figure 4: Sensitivity coefficient of reactions for a flow reactor (Initial conditions are $P$ = 1.0 atm, $T_i$ = 1080 K, $\phi \approx 3.4$, DME = 5160 ppm in $N_2$ for 80 % fuel consumed).

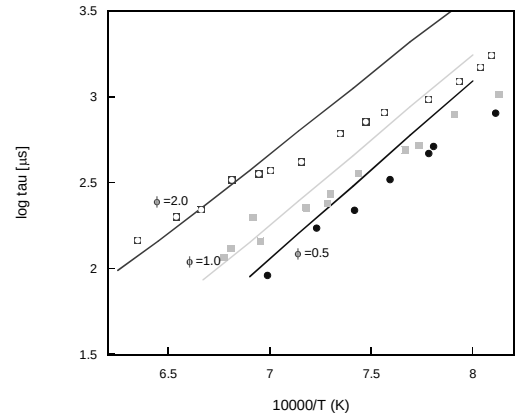


Figure 5: Comparison of experimental (symbols) and computed (lines) ignition delay times for DME. Mixture compositions used in the experiments: 1.0% DME-$O_2$-Ar, $P$ = 3.5 Bar [4].

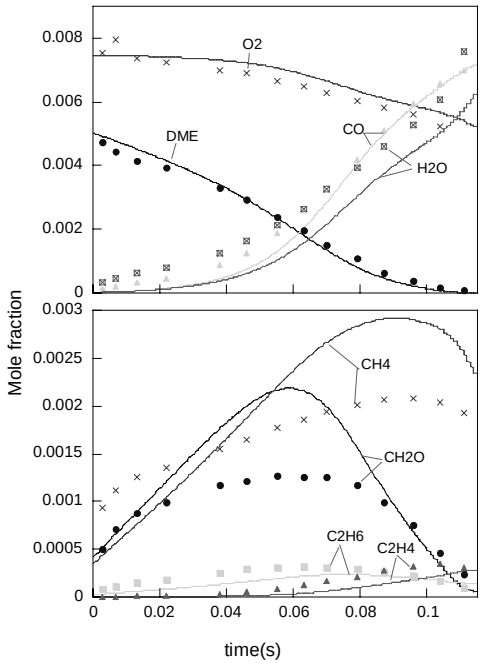


Figure 2: Comparison of experimental [2] (symbols) and computed (lines) species profiles during DME oxidation in a flow reactor ($P$ = 1.0 atm, $T_i$ = 1084 K, $\phi \approx 1.06$, initial DME concentration 5270 ppm in $N_2$). Model predictions are shifted by 11.6 ms.

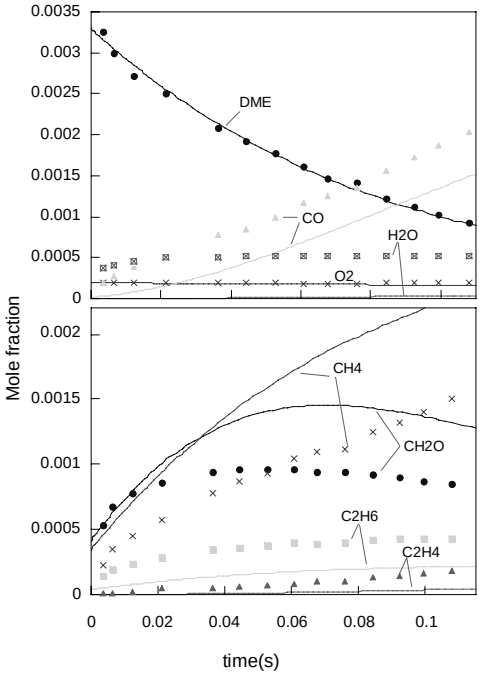


Figure 3: Comparison of experimental [2] (symbols) and computed (lines) species profiles during DME near-pyrolysis in a flow reactor ($P$ = 1.0 atm, $T_i$ = 1118 K, initial DME concentration 3740 ppm in $N_2$, $O_2$ concentration 190 ppm). Model predictions are shifted by 11.0 ms.

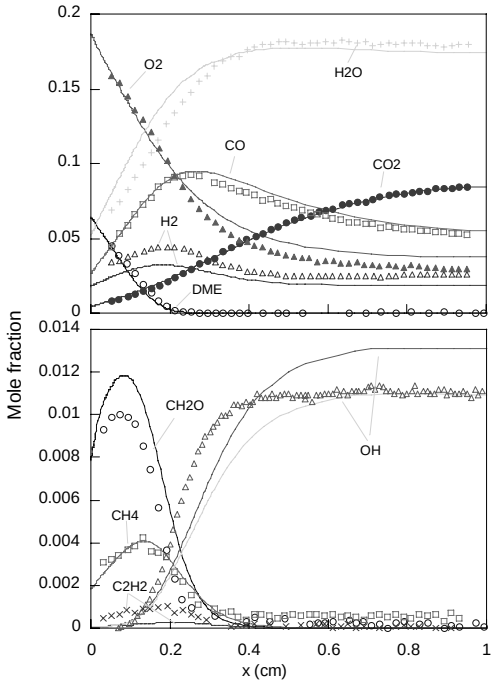


Figure 6: Comparison of experimental (McIlroy et al., 2000) (symbols) and computed (lines) species profiles in DME-$O_2$-Ar burner stabilized flame ($P$ = 40 kPa, $\phi$ = 0.98).

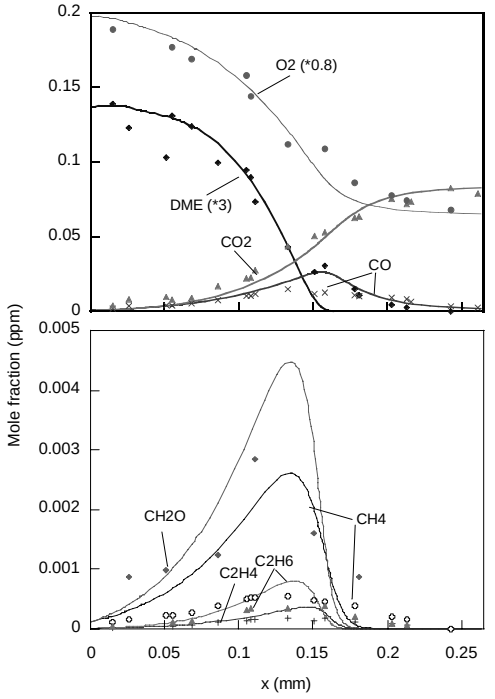


Figure 7: Comparison of experimental (Kaiser et al., 2000) (symbols) and computed (lines) species profiles in DME-Air burner stabilized flame ($P$ = 1.0 atm, $\phi$ = 0.67).

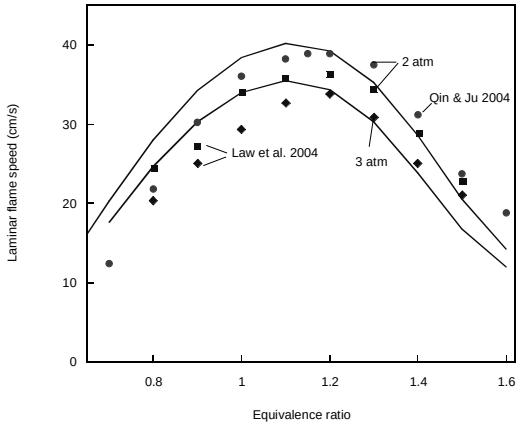


Figure 8: Laminar flame speed of DME/air mixtures at different pressure (2 and 3 atm). Symbols represent the experimental data of Qin & Ju (2004) and Law et al. (2004); line: model prediction.

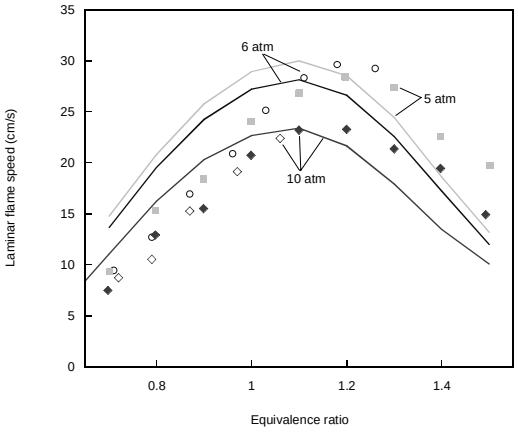


Figure 9: Laminar flame speed of DME/air mixtures at different pressure (5, 6 and 10 atm). Symbols represent the experimental data (open symbol: Qin & Ju 2004, solid: Law et al. 2004); line: model prediction.

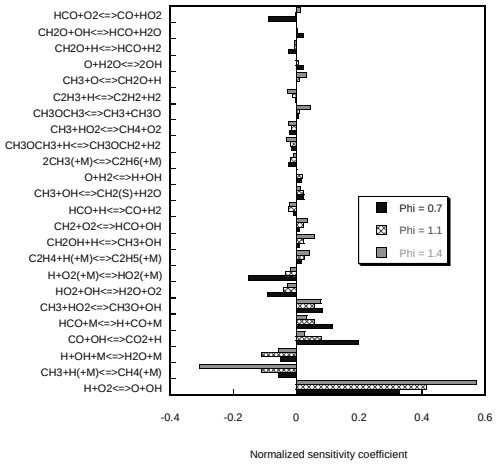


Figure 10: Normalized sensitivity coefficients of DME/air flame speeds at 298 K and 10 atm calculated using the present kinetic model.